Applied Catalysis B: Environmental 96 (2010) 449–457

Contents lists available at ScienceDirect

Applied Catalysis B: Environmental

journal homepage: www.elsevier.com/locate/apcatb

Influence of preparation method on the catalytic activities of $CuO/Ce_{0.67}Zr_{0.33}O_2$ catalysts in $CO + O_2$ reaction

Jie Zhu [a], Lingling Zhang [a], Yu Deng [b], Bin Liu [a], Lihui Dong [a], Fei Gao [b,*], Keqin Sun [c], Lin Dong [a,b,**], Yi Chen [a]

[a] Key Laboratory of Mesoscopic Chemistry of MOE, School of Chemistry and Chemical Engineering, Nanjing University, Nanjing 210093, PR China
[b] Center of Modern Analysis, Nanjing University, Nanjing 210093, PR China
[c] School of Energy and Environment, Southeast University, Nanjing 211102, PR China

ARTICLE INFO

Article history:
Received 4 November 2009
Received in revised form 1 March 2010
Accepted 2 March 2010
Available online 9 March 2010

Keywords:
CeO_2–ZrO_2 solid solution
Hydrothermal method
Preferentially exposed plane
"Incorporation Model"

ABSTRACT

$Ce_{0.67}Zr_{0.33}O_2$ solid solutions synthesized by traditional co-precipitation method (hereafter donated as CZ-CP) and hydrothermal method (hereafter donated as CZ-HT) were used as supports for preparing a series of $CuO/Ce_{0.67}Zr_{0.33}O_2$ catalysts. High resolution transmission electron microscopy (HRTEM), X-ray diffraction (XRD), temperature-programmed reduction (TPR), CO adsorption in situ Fourier transform infrared spectroscopy (CO in situ FT-IR) and the activity of CO oxidation model reaction at low temperature (<200 °C) were used to approach the properties of the catalysts. The results showed that the $Ce_{0.67}Zr_{0.33}O_2$ prepared by hydrothermal method facilitate the formation and stabilization of Cu^+ on the surface of support and thus the activity for $CO + O_2$ reaction was improved. A tentative model was suggested that the difference in the preferentially exposed plane of CZ-CP and CZ-HT leads to the great difference in dispersion, reduction and reaction activity of the dispersed copper oxide species on these two supports.

1. Introduction

Three-way catalysts (TWCs) have been widely investigated for their efficiency in controlling pollutant emissions from gasoline engine [1–3]. Among TWC catalysts, ceria-containing materials are now receiving remarkably increasing interest due to their significant applications in TWCs for its unique redox properties and high oxygen storage capacity (OSC), which are crucial for controlling the ratio of oxidants and reductants in automotive exhaust (NO_x, CO, hydrocarbons, etc.) [3–6]. However, as a support, ceria will result in significant efficiency decrease of the catalysts under thermally harsh environments, such as loss of surface area of the support, sintering of precious metals and deactivation of ceria [7–9]. Hence, CeO_2–ZrO_2 mixed oxides have gradually replaced pure CeO_2 as oxygen storage capacity (OSC) materials in the TWCs to reduce the emission of toxic pollutants from automobile exhaust, due to their enhanced reduction behavior and improved thermal stability at elevated temperatures [9–12].

So far, many techniques including high energy ball milling [13], co-precipitation [14], sol–gel [15], microwave [16] and hydrothermal synthesis [17] have been developed to synthesize CeO_2–ZrO_2 materials. Among these methods, hydrothermal synthesis has received more attention in scientific researches as it always offers an extraordinary merit in preparing highly crystallized nanomaterials with controlled shape, size and orientation. For example, Zhang and Yan reported that homogeneous nanostructured CeO_2–ZrO_2 solid solution could be prepared by the hydrothermal urea hydrolysis method [18,19].

Although CeO_2–ZrO_2 solid solution supported catalysts have been widely investigated, the dispersion and coordination state of active species are still not very clear. The interaction between metal oxide and oxide support has been investigated by many groups and some useful models have been proposed [20–22]. Based on a large amount of work and related literatures, "Incorporation Model" was proposed by our group in early 1990s [23] and has been used as an effective theory for explaining the dispersion and coordination state of various metal oxides on different supports [24–32]. According to this model, the supports are supposed to have a preferentially exposed plane. For example, ceria crystallizes in a cubic fluorite structure and exposes the thermodynamically most stable (1 1 1) surface [33]. Friedrich et al. have reported the high-resolution scanning tunneling microscopy results on CeO_2 (1 1 1) [34]. Primet et al. considered that the exposed plane are (0 0 1)

* Corresponding author at: Center of Modern Analysis, Nanjing University, Nanjing 210093, PR China. Tel.: +86 25 83592290; fax: +86 25 83317761.
** Corresponding author at: Key Laboratory of Mesoscopic Chemistry of MOE, School of Chemistry and Chemical Engineering, Center of Modern Analysis, Nanjing University, Nanjing 210093, PR China. Tel.: +86 25 83592290; fax: +86 25 83317761.
E-mail addresses: gaofei@nju.edu.cn (F. Gao), donglin@nju.edu.cn (L. Dong).

0926-3373/$ – see front matter © 2010 Elsevier B.V. All rights reserved.
doi:10.1016/j.apcatb.2010.03.003

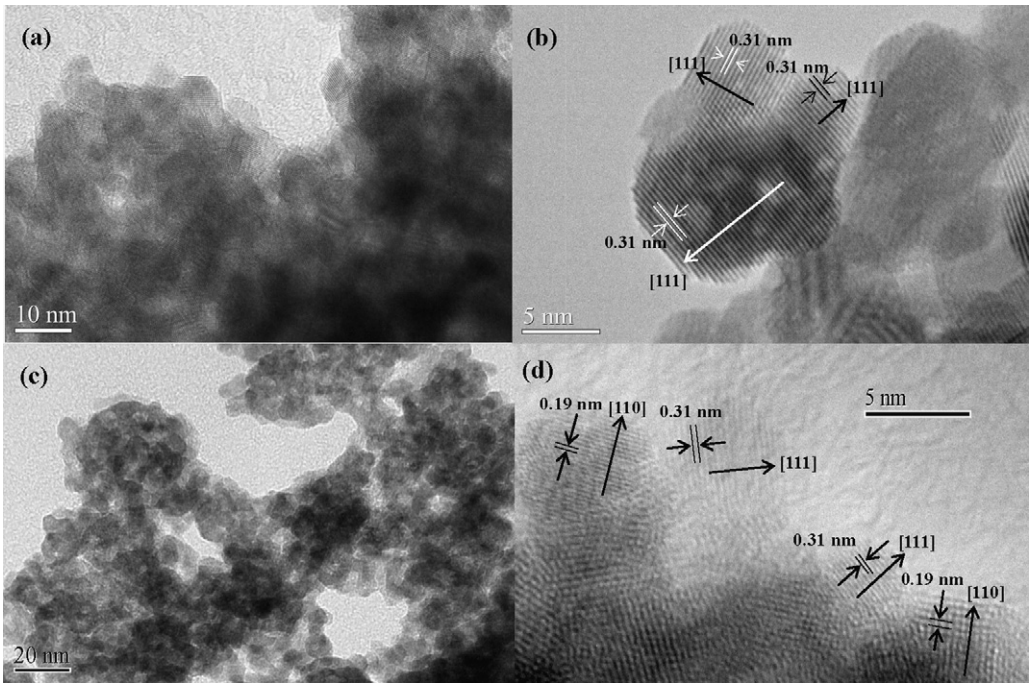

Fig. 1. TEM images of Cu/CZ-CP sample with (a) low resolution and (b) high resolution, and Cu/CZ-HT sample with (c) low resolution and (d) high resolution.

plane for the anatase TiO_2 and (1 1 0) plane for the rutile TiO_2 [35]. In the work of Jimenéz-Conzaléz et al., it was concluded by determination of lattice constant that most of the grains (~90%) of γ-alumina thin film are oriented with the surface normal along the (1 1 0) direction [36]. When metal oxides (e.g., CuO, NiO, etc.) are dispersed on the supports (e.g., Al_2O_3, CeO_2, TiO_2, ZrO_2, etc.), the ionic compounds are proceeded by the incorporation of the metal cations into the surface vacant sites on the support provided that the loading amounts of the compounds are not higher than their dispersion capacities. The dispersion capacity of supported catalysts deduced from the "Incorporation Model" is well consistent with the independent experiments and some chemical characters (e.g., reduction, adsorption and catalytic character) of the catalysts are also well explained [20–27].

In this work, $Ce_{0.67}Zr_{0.33}O_2$ solid solutions were synthesized by hydrothermal and co-precipitation methods respectively and then used as supports for a series of CuO catalysts. Different properties of these two kinds of catalysts such as dispersion, reduction, CO adsorption and the catalytic activity of $CO + O_2$ reaction were manifested. Deducing from "Incorporation Model", we proposed that the preferentially exposed plane of the $Ce_{0.67}Zr_{0.33}O_2$ solid solution prepared by co-precipitation method is (1 1 1) plane while that prepared by hydrothermal method should be (1 1 0) plane. On this basis, the different properties of these two kinds of catalysts were also explained.

2. Experimental

2.1. Sample preparation

$Ce_{0.67}Zr_{0.33}O_2$ solid solutions (denoted as CZ) were prepared by traditional co-precipitation method (CP) and hydrothermal method (HT), respectively.

CZ-CP support: $Ce(NO_3)_3$ and $Zr(NO_3)_4$ solutions with a molar ratio of Ce/Zr = 0.67:0.33 were mixed and stirred for 1 h. Then ammonium hydroxide solution (25 wt% ammonia) was added to the mixed solution until the pH value reached 10. The precipitation was kept at 100 °C for 12 h and then calcined in air at 550 °C for 6 h. The BET surface area of CZ-CP was 58 m^2/g.

CZ-HT support: an appropriate amount of $Ce(NO_3)_3$, $Zr(NO_3)_4$ and urea solution were mixed into the flask and stirred at 80 °C for 72 h. The molar ratio of Ce:Zr:urea was 0.67:0.33:2.5. The total concentration of Ce and Zr ions was 0.1 mol L^{-1}. The resulting solution was put into the Teflon autoclave and maintained at 120 °C for another 24 h. The resultant light yellow precipitant was collected, washed thoroughly with distilled water and absolute ethanol for several times, and then dried at 100 °C in air for 12 h. The as-prepared product was then calcined in air at 550 °C for 6 h with the elevation 1 °C min^{-1}. The BET surface area of as-prepared CZ-HT was 127 m^2/g.

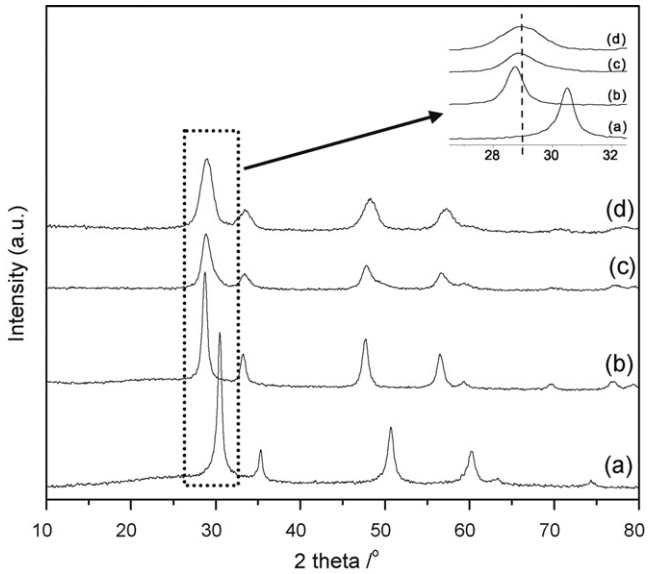

Fig. 2. XRD patterns of CZ samples (a) *t*-ZrO_2, (b) CeO_2, (c) CZ-CP and (d) CZ-HT.

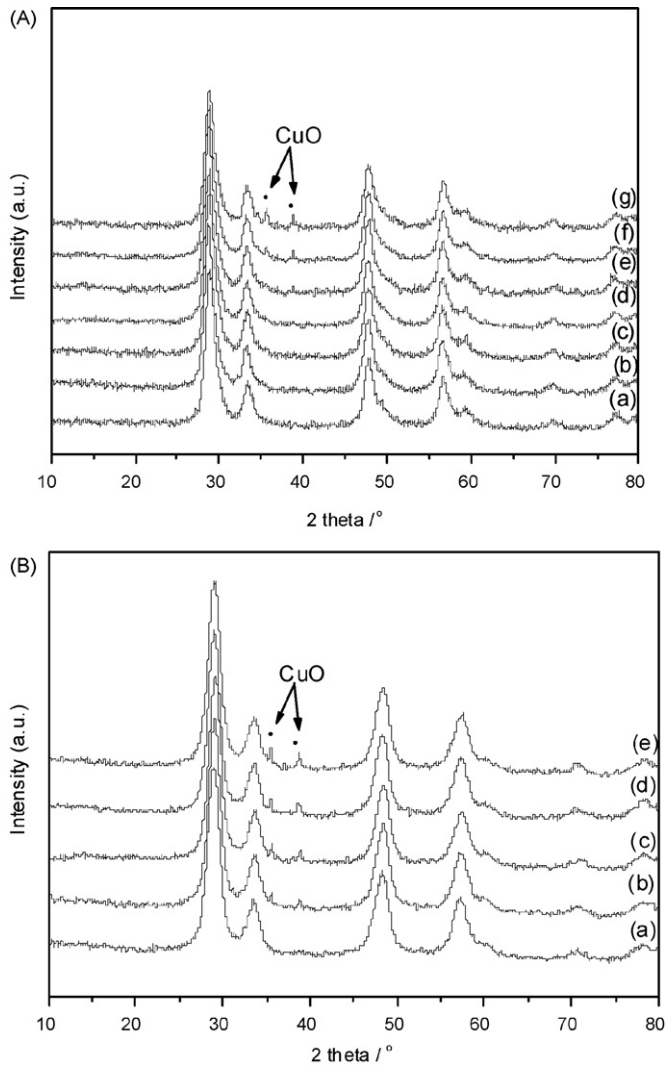

Fig. 3. The XRD patterns of (A) CZ-CP supported CuO catalysts with CuO loading: (a–g) 0.3, 0.6, 0.9, 1.2, 1.8, 2.4, 3.0 mmol/100 m^2, respectively and (B) CZ-HT supported CuO catalysts with CuO loading: (a–e) 0.48, 0.95, 1.27, 1.59, 1.91 mmol/100 m^2, respectively.

The CuO/CZ samples were prepared by impregnating CZ supports with an aqueous solution containing required amounts of $Cu(NO_3)_2$. Then the samples were dried at 100 °C for 12 h. After that, the samples were calcined in air at 450 °C for 5 h with the elevation 1 °C min^{-1}. The samples are denoted as xCu/CZ-CP and xCu/CZ-HT, respectively, e.g., 0.3Cu/CZ-CP corresponds to the CuO supported on CZ-CP support with the CuO loading amount at 0.3 mmol/100 m^2. The CuO loadings of Cu/CZ-CP samples were 0.3, 0.6, 0.9, 1.2, 1.8, 2.4, 3.0 mmol/100 m^2, respectively. The CuO loadings of Cu/CZ-HT samples were designed to be 0.3, 0.6, 0.8, 1.0, 1.2, respectively. After calcination, the BET surface area of Cu/CZ-HT samples reduced to about 80 m^2/g (while that of Cu/CZ-CP has no obvious change), due to the collapse of interparticle porous structure of CZ-HT support (see supplementary material 1). Thus, the actual CuO loadings were 0.48, 0.95, 1.27, 1.59, 1.91 mmol/100 m^2, respectively.

2.2. Characterization

The size and morphology of all of the samples were measured with a JEOL JEM-2100 high resolution transmission electron microscope (HRTEM).

X-ray diffraction (XRD) patterns were obtained with a Philips X'pert Pro diffractometer using Ni filtered Cu Kα radiation (0.15418 nm). The X-ray tube was operated at 40 kV and 40 mA.

Brunauer–Emmett–Teller (BET) surface area was measured by nitrogen adsorption at 77 K on a Micromeritics ASAP-2020 adsorption apparatus.

Temperature-programmed reduction (TPR) was carried out in a quartz U-tube reactor, and 100 mg sample was used for each measurement. Before reduction, the sample was pretreated in N_2 stream at 100 °C for 1 h and then cooled to room temperature. After that, a H_2–Ar mixture (7% H_2 by volume) with a flow rate of 40 mL min^{-1} was switched on and the temperature was increased linearly at a rate of 10 °C min^{-1}. A thermal conductivity cell was used to detect the consumption of H_2 on stream.

The activity tests of the catalysts in "$CO + O_2$" reaction were measured in a flow micro-reactor with a gas composition of 1.6% CO, 20.8% O_2 and 77.6% N_2 by volume at a space velocity of 30,000 mL g^{-1} h^{-1}, 25 mg catalyst was used for each measurement. The catalysts were pretreated in a N_2 stream at 100 °C for 1 h before being switched to the reaction gas stream. Tail gas was analyzed using gas chromatograph with a TCD. Two columns for gas separation, the one packed with 13X molecular sieve (30–60 M) for separating O_2, N_2 and CO and the other packed with Porapak Q for separating CO_2.

In situ Fourier transform infrared spectroscopy (FT-IR) of CO adsorption was carried out on a Nicolet 5700 FT-IR instrument

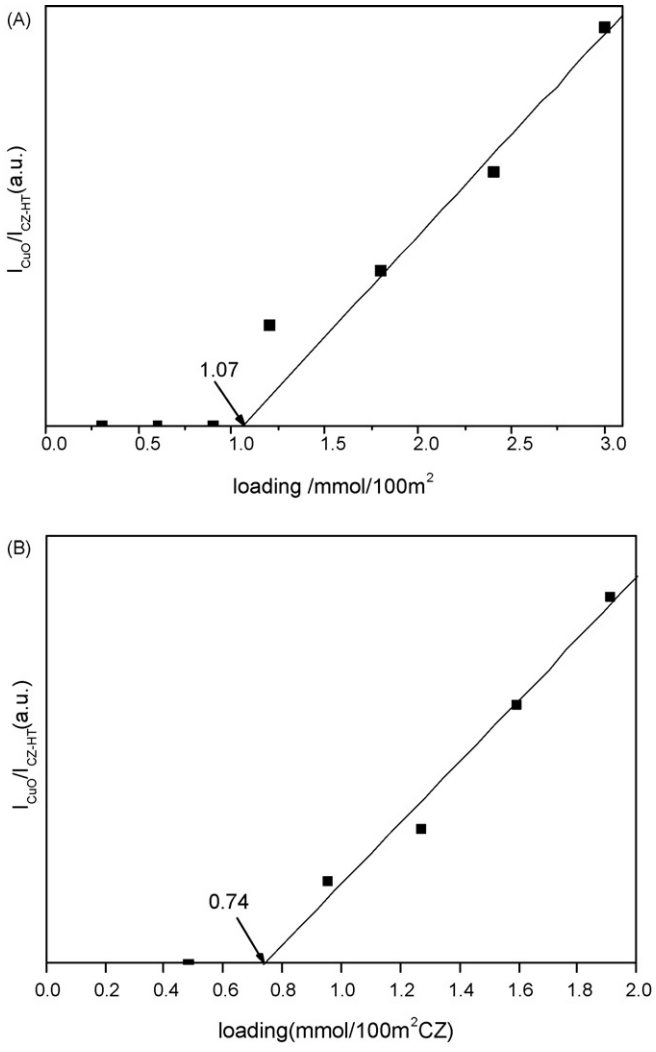

Fig. 4. Quantitative XRD results of (A) xCu/CZ-CP samples and (B) xCu/CZ-HT samples.

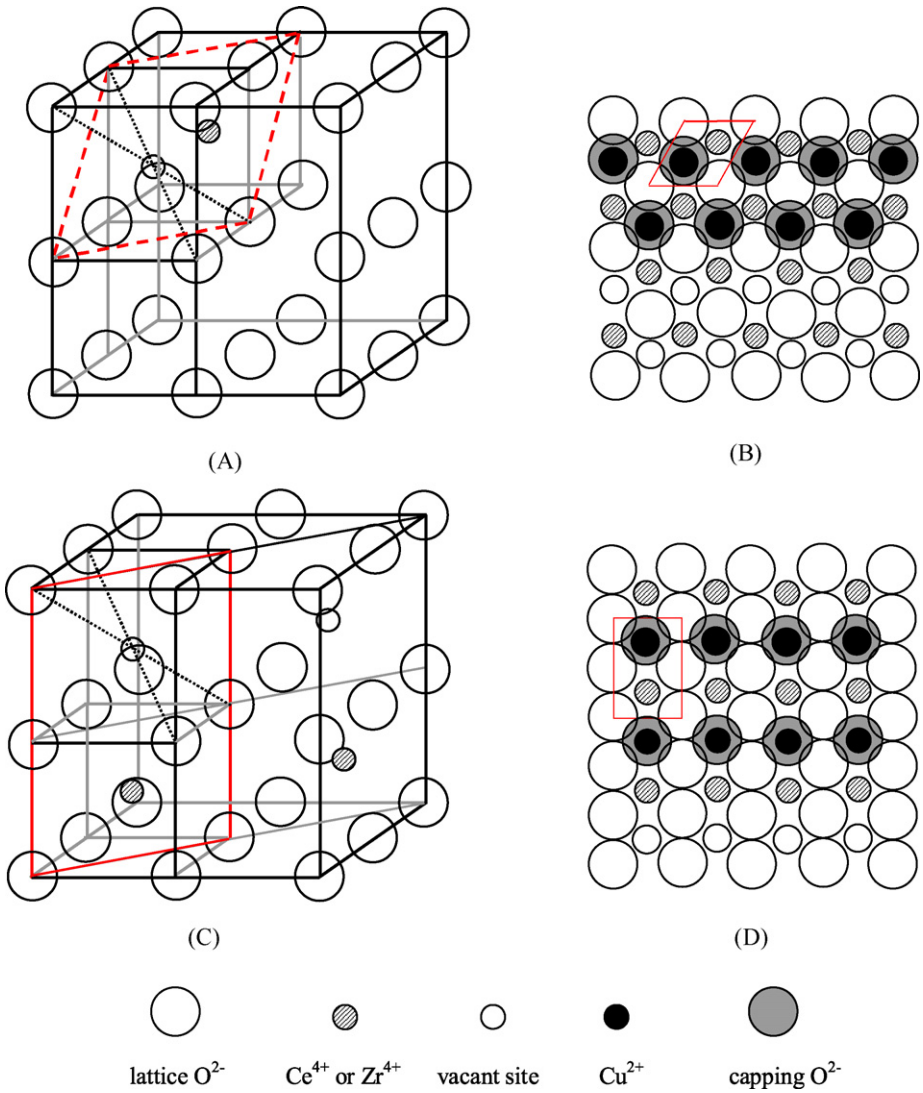

Fig. 5. Schematic diagram for the incorporated Cu^{2+} ions in the surface vacant sites of CZ supports: (A) the schematic diagram of crystal structure of CZ and its (1 1 1) plane, (B) incorporation of the dispersed Cu^{2+} species on the (1 1 1) plane of the CZ support, (C) the schematic diagram of crystal structure of CZ and its (1 1 0) plane and (D) incorporation of the dispersed Cu^{2+} species on the (1 1 0) plane of the CZ support.

(Thermo Electron Corporation, USA) running at 4 cm^{-1} resolutions. A thin, but intact, self-supporting wafer (≈15 mg) of the adsorbents was prepared and mounted inside a high temperature cell (HTC-3, Harrick Scientific Corporation, USA). The wafer was pretreated by N_2 (99.999%) at 400 °C for 1 h. After cooling to ambient temperature, CO–N_2 mixture (10% CO by volume) was introduced into the HTC at atmospheric pressure for 30 min, then the HTC was heated to 350 °C under CO atmosphere at a rate of 10 °C min^{-1} and the spectra were recorded at target temperatures.

3. Results and discussion

3.1. TEM

Fig. 1(a) and (b) shows the low and high resolution TEM images of CZ-CP sample, respectively. From the low magnification image (Fig. 1(a)), we can observe that the sample is not well dispersed and their grain sizes are in the range of 5–15 nm. To further investigate its crystal structure and exposed plane, the HRTEM image is presented in Fig. 1(b). Only one kind of periodicity of observed fringes (0.31 nm) can be observed, which is compatible with the distance expected between the (1 1 1) reticular planes of CZ. The result indicates that the growth direction of CZ-CP sample is mainly [1 1 1] and the preferentially exposed plane should be (1 1 1) plane for the sample prepared by co-precipitation method, which is consistent with our previous study [31]. On the other hand, the TEM images with low magnification of CZ-HT sample is given in Fig. 1(c). Similar to that of CZ-CP sample, the CZ-HT sample also consists of aggregated particles with irregular morphology and their grain sizes are about 5–15 nm. However, from the HRTEM image (Fig. 1(d)), it can be observed that the growth direction of CZ-HT sample is mainly [1 1 0] and [1 1 1], implying that the (1 1 0) and (1 1 1) planes are exposed outside for the hydrothermal prepared sample. Thus, we can conclude that the exposed planes should be mainly (1 1 0) and (1 1 1) planes in CZ-HT samples. However, as the morphology of CZ-HT sample is irregular, the relative amount of these two kinds of exposed planes is difficult to be distinguished by HRTEM.

3.2. XRD

Fig. 2 shows the XRD patterns of CZ-CP and CZ-HT samples. For comparison, the curves of pure CeO_2 and *t*-ZrO_2 are also listed. The results reveal that both samples are Ce–Zr solid solution with cubic fluorite structures and the lattice parameter obtained from the cal-

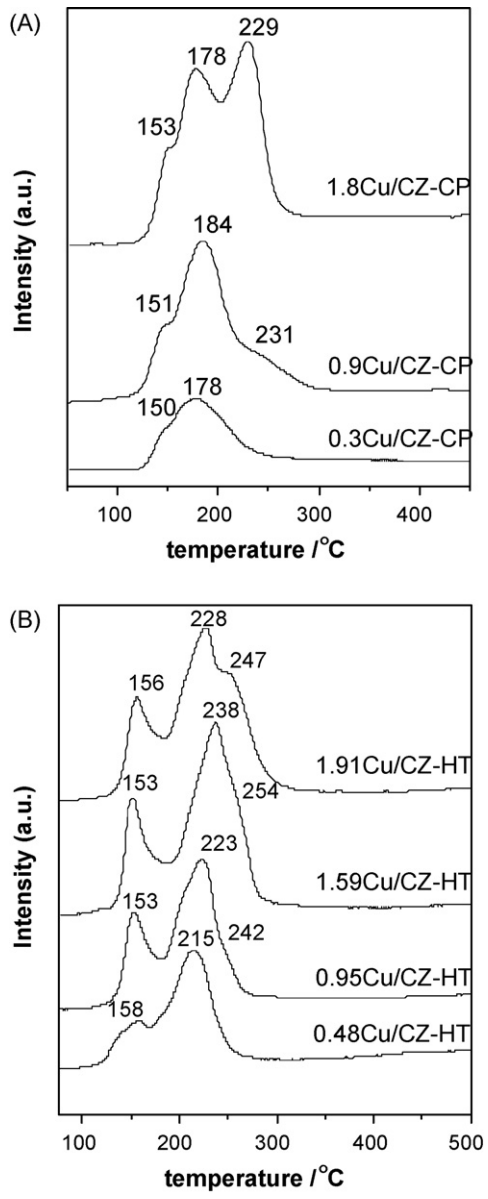

Fig. 6. TPR profiles of (A) some xCu/CZ-CP samples with CuO loading 0.3, 0.9 and 1.8 mmol/100 m^2, respectively and (B) some xCu/CZ-HT samples with CuO loading 0.48, 0.95, 1.59 and 1.91 mmol/100 m^2, respectively.

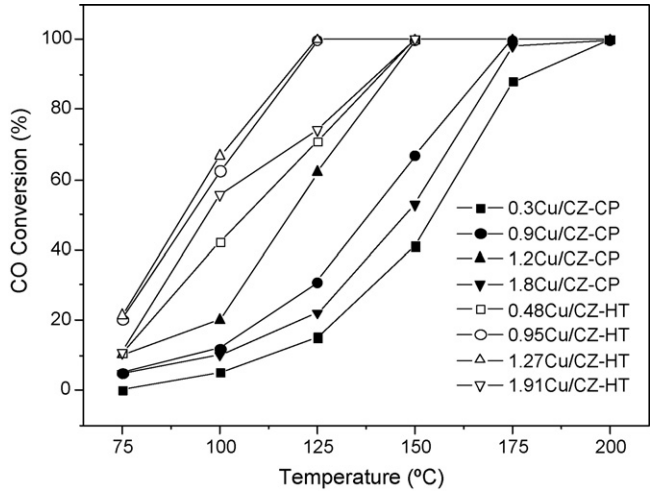

Fig. 7. The CO oxidation activity of xCu/CZ-HT and xCu/CZ-CP catalysts.

culation of (1 1 1) peak is about 0.535 nm, which is in agreement with the product of CZ obtained from other route [37].

XRD patterns of a series of Cu/CZ-CP and Cu/CZ-HT samples with different CuO loadings are presented in Fig. 3A and B, respectively. For Cu/CZ-CP samples with low CuO loadings (0.3, 0.6 and 0.9 mmol/100 m^2 CZ-CP), no crystalline peaks of copper oxides can be observed, as shown in Fig. 3A(a–c), which suggests that the copper species have been highly dispersed on the surface of CZ-CP. For samples with high CuO loadings ($\geq$1.2 mmol/100 m^2), the typical diffraction peaks of crystalline CuO ($2\theta = 35.5^\circ$ and 38.8°) have been found, as shown in Fig. 3A(d–g), and the intensities of these peaks increase with the CuO loadings, indicating the formation of crystalline CuO. Whereas, for Cu/CZ-HT samples (Fig. 3B), the characteristic peaks of crystalline CuO appear in 0.95, 1.27, 1.59 and 1.91Cu/CZ-HT samples, except for 0.48Cu/CZ-HT sample. Accordingly, XRD quantitative analysis results of both series samples are shown in Fig. 4. The dispersion capacities of copper oxide on CZ-CP and CZ-HT support are around 1.07 and 0.74 mmol/100 m^2 CZ, respectively. This result indicates that the surface structure of the two kinds of catalysts should be of great difference.

As we reported previously, the dispersion capacities of bivalent metal oxides (e.g., CuO, NiO, etc.) on the surface of various supports have been successfully explained by "Incorporation Model", e.g., CeO_2 [26], ZrO_2 [27], TiO_2 [28], Al_2O_3 [25,26] and some modified or complex oxide supports [16,29,30]. For CeO_2–ZrO_2 solid solution supported catalysts, the "Incorporation Model" is also applicable [16,31].

According to the literatures [31,38,39], both ceria and zirconia have fluorite structures. The (1 1 1) planes, which are thermodynamically most stable and have cubic vacant sites, are preferentially exposed on the surface of CeO_2 and ZrO_2. It is reasonable to suggest that the (1 1 1) plane is also preferentially exposed on the surface of CeO_2–ZrO_2 solid solution, which has a fluorite structure as well. This assumption is also supported by our HRTEM result. Thus, in the present work, the preferentially exposed plane of CZ-CP is considered to be (1 1 1) plane. The scheme of (1 1 1) plane of CZ-CP is shown in Fig. 5(A) and (B). Considering the lattice parameter of CZ-CP obtained from XRD results (0.535 nm), the vacancy density is calculated to be 1.34 mmol/100 m^2. When CZ-CP is impregnated by $Cu(NO_3)_2$ aqueous solution, the vacant sites on the surface of CZ-CP will be occupied by Cu^{2+} ions, so the dispersion capacity of CuO should be 1.34 mmol/100 m^2. The experimental dispersion capacity of CuO on the surface of CZ-CP is about 1.07 mmol/100 m^2, which is basically coincided with the theoretic value.

However, for Cu/CZ-HT samples, the dispersion capacity is only about 0.74 mmol/100 m^2, which has obvious difference with theoretic results of CuO dispersion on (1 1 1) plane of CZ (1.34 mmol/100 m^2). Based on our previous study [28], we tentatively discussed the possible reason by considering the shielding effect of accompanying NO_3^- anions, which may induce the dispersion capacity far below the theoretic values. When CZ-HT was impregnated by $Cu(NO_3)_2$ aqueous solution, Cu^{2+} ions would occupy the vacant sites on the surface of CZ-HT and the two accompanying NO_3^- anions would stay at the top of the occupied site as capping NO_3^-, compensating the extra positive charge. The two accompanying NO_3^- anions would prevent some of the neighboring vacant sites on the surface of CZ-HT. Along this line, the dispersion capacity of CuO on the surface of CZ-HT should be basically equal to the dispersion capacity of $Cu(NO_3)_2$ on CZ-HT. As reported in literature [40], the effect radius and area of NO_3^- is about 0.19 nm and 0.125 nm^2, respectively. Thus, the dispersion capacity can be calculated to be about 0.66 mmol/100 m^2, which is basically coincided with the XRD results. It seems that the lower dispersion capacity of CuO could be explained by the shielding effect of capping NO_3^- anions. However, the dispersion capacity should increase significantly through the double impregnation pro-

cessing. Actually, for our samples, the dispersion capacity after the double impregnation (see supplementary material 2) is only about 0.86 mmol/100 m^2, which has not obvious increment than that of one-step impregnation samples (0.74 mmol/100 m^2). Therefore, this assumption may not fit for Cu/CZ-HT samples in this work.

On the other hand, according to the literatures, the preparation method could affect the exposed plane of the support [38,41]. According to the "Incorporation Model", we calculated the surface vacant sites of some common lattice planes of CZ and found that if the (1 1 0) plane is considered as the preferentially exposed plane for CZ-HT support, as shown in Fig. 5(C) and (D), the density of surface vacant sites can be calculated to be 0.79 mmol/100 m^2, which also be the theoretical dispersion capacity of Cu^{2+} ions on the surface of CZ-HT support. This result matches the experimental results very well. Combined with the HRTEM results, it is reasonable to suppose the preferentially exposed plane of CZ-HT sample should be (1 1 0) plane.

3.3. H_2-TPR

Fig. 6(A) is the TPR curves of Cu/CZ-CP samples. For 0.3Cu/CZ-CP sample, two reductive peaks can be observed at about 155 °C and 180 °C, with the former peak appears as a shoulder. As discussed in XRD section, all the Cu species are well dispersed on the surface of CZ-CP in this sample. Thus the two peaks could be attributed to the stepwise reduction of dispersed CuO, i.e., $Cu^{2+} \rightarrow Cu^{+}$ and $Cu^{+} \rightarrow Cu^{0}$ [42]. When the CuO loading is 0.9 and 1.8 mmol/100 m^2 CZ-CP, a new reduction peak at about 230 °C appears, corresponding to the reduction of crystalline CuO [43,44]. However, for 0.9Cu/CZ-CP sample, the peak only appears as a weak shoulder, implying the crystalline CuO exists as small CuO cluster, which is not detectable for XRD characterization.

Fig. 6(B) is the TPR curves of Cu/CZ-HT samples. For 0.48Cu/CZ-HT sample, two reduction peaks corresponding to stepwise reduction of dispersed CuO appear at about 155 °C and 220 °C, respectively. When the CuO loading exceeds the dispersion capacity, the reduction of crystalline CuO appears at about 240 °C. For 0.95 and 1.59Cu/CZ-HT samples, the peaks of crystalline CuO only appear as shoulders, due to the overlap with the reduction peaks of $Cu^{+} \rightarrow Cu^{0}$.

Compared the TPR results of these samples, it can be observed that the reduction temperatures of $Cu^{2+} \rightarrow Cu^{+}$ for both series samples are almost the same (~150 °C). While the reduction temperature of $Cu^{+} \rightarrow Cu^{0}$ is about 45 °C disparities (180 °C for Cu/CZ-CP samples and 225 °C for Cu/CZ-HT samples), indicating that the Cu^{+} on the surface of CZ-HT surface are difficult to be reduced, i.e., the ceria–zirconia solid solution prepared by hydrothermal method has stabilization effect on dispersed Cu^{+} species.

3.4. Activity of $CO + O_2$ reaction

The activity tests for $CO + O_2$ reaction were performed for some Cu/CZ-CP and Cu/CZ-HT samples and the results are shown in Fig. 7. For both Cu/CZ-CP and Cu/CZ-HT samples, the activities for CO conversion have similar characters as we have reported previously [16]. When the Cu contents are below the dispersion capacity, the CO conversion increases with Cu loading. When the Cu loadings are much higher than the dispersion capacity, the CO conversion decreases dramatically. The results indicate that the dispersed Cu species are active for $CO + O_2$ reaction, while the bulk CuO particles hinder the process of the reaction, which is in accordance with the literature [45].

It also can be clearly observed that the activities of Cu/CZ-HT samples are obviously higher than that of Cu/CZ-CP ones. Contrasting 0.48Cu/CZ-HT and 0.9Cu/CZ-CP samples, in which all the Cu species are highly dispersed and the Cu content in 0.48Cu/CZ-HT (~3 wt%) is even lower than that in 0.9Cu/CZ-CP (~4 wt%), the turn over number of each Cu ion per hour at 125 °C is calculated to be 12.3 and 38.2 h^{-1}, respectively, indicating the activity of 0.48Cu/CZ-HT is about three times as high as that of 0.9Cu/CZ-CP sample.

As reported elsewhere, the CO adsorption is a necessary step in $CO + O_2$ reaction [46,47]. For supported CuO catalysts, as Cu^{0} and Cu^{2+} can absorb CO molecules only at extremely low temperature, the Cu^{+} species, which have obvious CO adsorption at ambient temperature, are considered to be active for $CO + O_2$ reaction. As discussed in TPR section, the CZ supports prepared by hydrothermal method facilitate the stabilization of Cu^{+} on the surface, thus the CuO catalysts supported on the CZ-HT should have much better activity than those supported on CZ-CP.

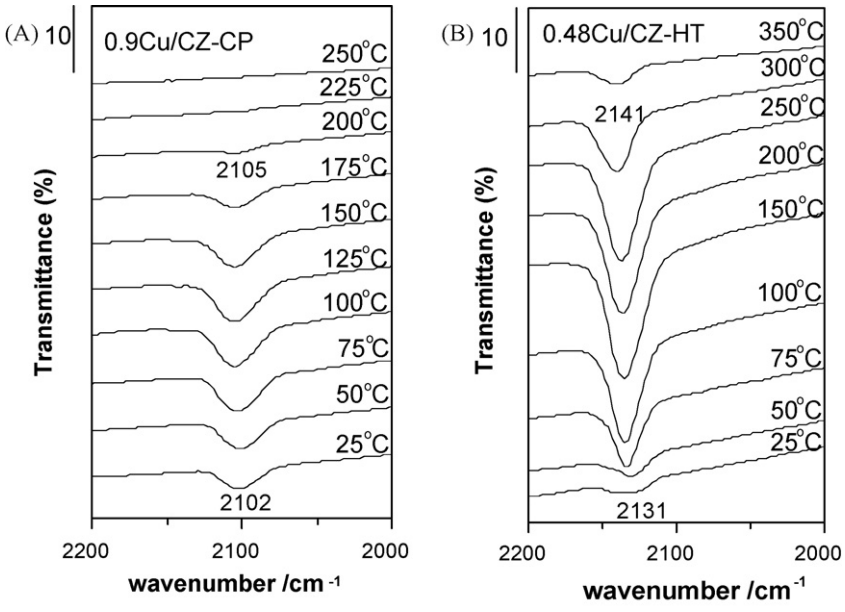

Fig. 8. In situ FT-IR spectra of CO adsorbed on (A) 0.9Cu/CZ-CP and (B) 0.48Cu/CZ-HT samples.

3.5. CO in situ FT-IR

To further explore the stabilization effects of support on the surface dispersed copper oxide species, the CO adsorption in situ FT-IR spectra of 0.48Cu/CZ-HT and 0.9Cu/CZ-CP samples are recorded, as shown in Fig. 8. Generally, the adsorption of CO molecules on Cu^{2+}, Cu^{+}, and Cu^{0} gives rise to peaks with characteristic vibrational frequencies at about 2220–2150 cm^{-1}, 2160–2080 cm^{-1}, and below 2130 cm^{-1}, respectively, and at the ambient temperature, Cu^{+}–CO is most stable adsorption [48–51]. As the support has no CO adsorption at 2200–2050 cm^{-1} region, the peak at about 2110 cm^{-1} in the spectra should be attributed to the vibration of Cu^{+}–CO. It can be observed that there are similar characters in FT-IR spectra for both samples. The peaks of CO adsorption on the Cu^{+} are evident at room temperature and with the elevation of temperature, the peak intensities increase gradually to maximum and then decrease until disappearance. The Cu^{+}–CO adsorption peaks at room temperature indicate that there are some Cu^{+} species in the samples at ambient temperatures. With the temperature increasing, the Cu species are reduced gradually and more Cu^{+} ions form on the surface of CZ support, thus the peak intensity increases gradually to maximum. As the temperature increases continuously, Cu^{+} are further reduced to Cu^{0} and the peak intensity decreases gradually until disappearance. However, the desorption temperatures of Cu^{+}–CO peaks are greatly different for 0.48Cu/CZ-HT and 0.9Cu/CZ-CP samples. For 0.9Cu/CZ-CP sample (Fig. 8(A)), the maximum peak area of CO adsorption on Cu^{+} appears at about 100 °C and disappears completely at 225 °C. Compared with 0.9Cu/CZ-CP sample, the CO adsorption reaches maximum at about 150 °C for 0.48Cu/CZ-CP (Fig. 8(B)) and the desorption process is very slow, which can be observed even at 350 °C. It can be concluded that the CO adsorption on Cu/CZ-HT is much more stable than Cu/CZ-CP, i.e., the Cu^{+} is much more stable in Cu/CZ-HT than that in Cu/CZ-CP.

Considering the difference in preferentially exposed plane of these two supports, the following explanation is suggested. For CZ-CP samples, the (1 1 1) plane is preferentially exposed on the surface. As the lattice parameter of CZ-CP is 0.535 nm, the maximal radius that the vacant sites can accommodate is about 77 pm. The Cu^{2+}, with radius about 73 pm, could totally incorporate into the

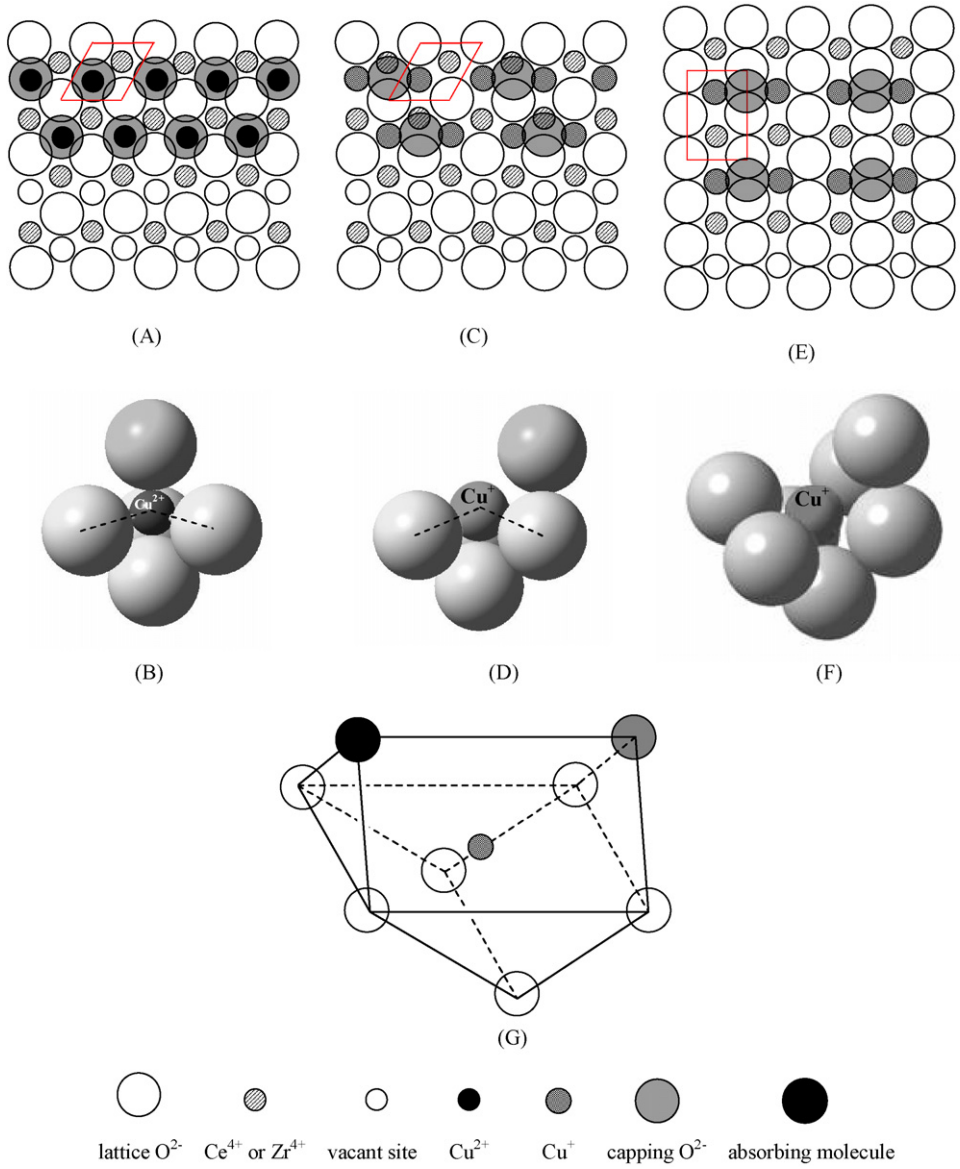

Fig. 9. The schematic model of (A) and (B) Cu^{2+} incorporated in the (1 1 1) surface of the CZ, (C) and (D) Cu^{+} incorporated in the (1 1 1) surface of CZ and (E) and (F) Cu^{+} incorporated in the (1 1 0) surface of CZ. (G) The model of coordinative environment of Cu^{+} on the (1 1 0) surface.

vacant sites. Meanwhile, the capping oxygen covers on the top of the Cu^{2+}, which forms a penta-coordinative environment of Cu^{2+} (Fig. 9(A) and (B)). When Cu^{2+} is reduced to Cu^{+}, the dispersion states of Cu^{+} could be schemed as Fig. 9(C). As the radius of Cu^{+} (96 pm) is larger than the size of the vacancy (77 pm), the Cu^{+} could not totally incorporate into the vacancy, i.e., the Cu^{+} should be slightly elevated and "float" above the plane of surface lattice oxygen anions, as shown in Fig. 9(D), which increase the exposed area of Cu^{+} than Cu^{2+} in Fig. 9(B). It also can be seen that each capping oxygen anion is shared by two Cu^{+} cations, thus the Cu^{+} locates in an asymmetric penta-coordinative environment, which is a much more unstable structure than the coordinative environment of Cu^{2+}. Therefore, the Cu^{+} is easier to be attacked by reductive molecules than Cu^{2+}. Hence, when the Cu^{2+} is reduced to Cu^{+}, the Cu^{+} could be successively reduced to Cu^{0} species immediately.

While for CZ-HT samples, the preferentially exposed plane is supposed to be (1 1 0) plane. The maximal radius that the vacancies can accommodate is calculated to be 98 pm, which is larger than the radius of Cu^{2+} (73 pm) and Cu^{+} (96 pm). Therefore, the Cu^{+} could totally incorporate into the surface vacancies, as shown in Fig. 9(E) and (F). The Cu^{+} ion is surrounded by seven oxygen anions to form a defective octahedral copper oxide species. However, after absorbing reductive molecules, the coordination of Cu^{+} forms an octahedral environment (Fig. 9(G)), which is a stable symmetric structure, thus the Cu^{+} should be easy to attach reductive molecules but difficult to be reduced to Cu^{0}. Thus, the CO absorption peaks on Cu^{+} in FT-IR spectra are fairly strong in a wide temperature range for Cu/CZ-HT sample. The model indicates that the Cu^{+} in CZ-HT samples are more stable than in CZ-CP samples, which is in accordance with the TPR, reaction test and CO in situ FT-IR results.

4. Conclusions

The different preparation methods of CeO_2–ZrO_2 solid solution may lead to the different preferentially exposed planes. In this work, the preferentially exposed plane of CZ sample prepared by conventional co-precipitation method is (1 1 1) plane, while that of CZ sample prepared by hydrothermal method should be (1 1 0) plane, which leads to the following different properties for the two kinds of supported CuO catalysts:

1. The dispersion capacity of CuO on the surface of CZ-CP is about 1.07 mmol/100 m^2, while the dispersion capacity is 0.74 mmol/100 m^2 for CZ-HT supported CuO catalysts. The vacancy density on (1 1 0) plane is lower than that on (1 1 1) plane, thus the dispersion capacity of Cu/CZ-HT is much less than Cu/CZ-CP samples.
2. The coordinative environment of reduced Cu^{+} dispersed on (1 1 1) plane is a highly distorted penta-coordinative structure, while the coordinative environment of reduced Cu^{+} dispersed on (1 1 0) plane forms a stable symmetrical octahedral structure after absorbing a reductive molecule. Thus, the surface structure of CZ prepared by hydrothermal method is easier to absorb micro molecules and facilitate the stabilization Cu^{+} on the surface of support, which promotes the activity in $CO + O_2$ reaction significantly.

Acknowledgements

The financial supports of the National Natural Science Foundation of China (Nos. 20873060, 20973091), the Project of Jiangsu innovation talent (BK2008001) and the National Basic Research Program of China (2010CB732300) are gratefully acknowledged.

Appendix A. Supplementary data

Supplementary data associated with this article can be found, in the online version, at doi:10.1016/j.apcatb.2010.03.003.

References

[1] I. Heo, J.W. Choung, P.S. Kim, I.-S. Nam, Y.I. Song, C.B. In, G.K. Yeo, Appl. Catal. B: Environ. 92 (2009) 114–125.
[2] H. Birgersson, L. Eriksson, M. Boutonnet, S.G. Järås, Appl. Catal. B: Environ. 54 (2004) 193–200.
[3] J.R. González-Velasco, M.A. Gutiérrez-Ortiz, J.-L. Marc, J.A. Botas, M.P. González-Marcos, G. Blanchard, Appl. Catal. B: Environ. 25 (2000) 19–29.
[4] R. Burch, J.P. Breen, F.C. Meunier, Appl. Catal. B: Environ. 39 (2002) 283–303.
[5] J.C. Chen, M.Y. Wey, C.L. Yeh, Y.S. Liang, Appl. Catal. B: Environ. 48 (2004) 25–35.
[6] K. Yamazaki, N. Takahashi, H. Shinjoh, M. Sugiura, Appl. Catal. B: Environ. 53 (2004) 1–12.
[7] J. Kašpar, P. Fornasiero, M. Graziani, Catal. Today 50 (1999) 285–298.
[8] J. Kašpar, P. Fornasiero, N. Hickey, Catal. Today 77 (2003) 419–449.
[9] S.P. Wang, X.C. Zheng, X.Y. Wang, S.R. Wang, S.M. Zhang, L.H. Yu, W.P. Huang, S.H. Wu, Catal. Lett. 105 (2005) 163–168.
[10] L.F. Liotta, A. Macaluso, A. Longo, G. Pantaleo, A. Martorana, G. Deganello, Appl. Catal. A: Gen. 240 (2003) 295–307.
[11] N. Kakuta, S. Ikawa, T. Eguchi, K. Murakami, H. Ohkita, T. Mizushima, J. Alloys Compd. 408–412 (2006) 1078–1083.
[12] G. Larese, M.L. Granados, R. Mariscal, J.L.G. Fierro, P.S. Lambrou, A.M. Efstathiou, Appl. Catal. B: Environ. 59 (2005) 13–25.
[13] A. Trovarelli, F. Zamar, J. Llorca, C.D. Leitenburg, G. Dolcetti, J.T. Kiss, J. Catal. 169 (1997) 490–502.
[14] S. Pengpanich, V. Meeyoo, T. Rirksomboon, K. Bunyakiat, J. Catal. A: Gen. 234 (2002) 221–233.
[15] J. Kašpar, P. Fornasiero, G. Balducci, R. Di Monte, N. Hickey, V. Sergo, Inorg. Chim. Acta 349 (2003) 217–226.
[16] H.L. Chen, H.Y. Zhu, Y. Wu, F. Gao, L. Dong, J.J. Zhu, J. Mol. Catal. A 255 (2006) 254–259.
[17] M. Hirano, T. Miwa, M. Inagaki, J. Am. Ceram. Soc. 84 (2001) 1728–1732.
[18] R. Si, Y.W. Zhang, C.X. Xiao, S.J. Li, B.X. Lin, Y. Kou, C.H. Yan, Phys. Chem. Chem. Phys. 6 (2004) 1056–1063.
[19] R. Si, Y.W. Zhang, S.J. Li, B.X. Lin, C.H. Yan, J. Phys. Chem. B 108 (2004) 12481–12488.
[20] H. Knozinger, Proc. 9th ICC, Calgary, 1988.
[21] I.E. Wachs, R.Y. Saleh, S.S. Chan, C.C. Chersich, Appl. Catal. 15 (1985) 339–352.
[22] Y.C. Xie, Y.Q. Tang, Adv. Catal. 37 (1990) 1–43.
[23] Y. Chen, L. Zhang, Catal. Lett. 12 (1992) 51–62.
[24] Z. Wang, H.Q. Wan, B. Liu, X. Zhao, X.W. Li, H.Y. Zhu, X. Xu, F.Y. Ji, K.Q. Sun, L. Dong, Y. Chen, J. Colloid Interface Sci. 320 (2008) 520–526.
[25] H.Q. Wan, Z. Wang, J. Zhu, X.W. Li, B. Liu, F. Gao, L. Dong, Y. Chen, Appl. Catal. B: Environ. 79 (2008) 254–261.
[26] Y. Chen, L. Dong, Y.S. Jin, Stud. Surf. Sci. Catal. 101 (1996) 1293–1302.
[27] Z. Liu, W.J. Ji, L. Dong, Y. Chen, J. Catal. 172 (1997) 243–246.
[28] H.Y. Zhu, Y. Wu, X. Zhao, H.Q. Wan, J.M. Hong, Q. Yu, L. Dong, Y. Chen, J. Mol. Catal. A 243 (2006) 24–30.
[29] J. Wang, L. Dong, Y.H. Hu, G.S. Zheng, Z. Hu, Y. Chen, J. Solid State Chem. 157 (2001) 274–282.
[30] H.Y. Zhu, M.M. Shen, Y. Kong, Y.H. Hu, T.D. Liu, L. Dong, Y. Chen, C. Jian, Z. Liu, J. Mol. Catal. A 219 (2004) 155–164.
[31] X.W. Li, M.M. Shen, X. Hong, H.Y. Zhu, F. Gao, Y. Kong, L. Dong, Y. Chen, J. Phys. Chem. B 109 (2005) 3949–3955.
[32] B.M. Reddy, B. Chowdhury, E.P. Reddy, A. Fernández, J. Mol. Catal. A 162 (2000) 431–441.
[33] A. Trovarelli (Ed.), Catalysis by Ceria and Related Materials, Imperial College Press, London, 2002.
[34] F. Esch, S. Fabris, L. Zhou, T. Montini, C. Africh, P. Fornasiero, G. Comelli, R. Rosei, Science 309 (2005) 752–755.
[35] M. Primet, P. Pichat, M.-V. Mathieu, J. Phys. Chem. 75 (1971) 1216–1220.
[36] A. Jimenez-Gonzalez, D. Schmeisser, Surf. Sci. 250 (1991) 59–70.
[37] A. Martínez-Arias, M. Fernández-García, V. Ballesteros, L.N. Salamanca, J.C. Conesa, J.C. Conesa, C. Otero, J. Soria, Langmuir 15 (1999) 4796–4802.
[38] H.D. Cochrane, J.L. Hutchison, D. White, Ultramicroscopy 31 (1989) 138–142.
[39] Z. Liu, Y. Chen, J. Catal. 177 (1998) 314–324.
[40] J.T. Cheng, P.D. Ellis, J. Phys. Chem. 93 (1989) 2549–2555.
[41] K.B. Zhou, X. Wang, X.M. Sun, Q. Peng, Y.D. Li, J. Catal. 229 (2005) 206–212.
[42] P. Zimmer, A. Tschöpe, R.J. Birringer, J. Catal. 205 (2002) 339–345.
[43] X. Zheng, X. Zhang, S. Wang, X. Wang, S. Wu, J. Nat. Gas Chem. 16 (2007) 179–185.
[44] G.R. Rao, H.R. Sahu, B.G. Mishra, Colloid Surf. A: Physicochem. Eng. Aspects 220 (2003) 261–269.
[45] A. Martínez-Arias, M. Fernández-García, A.B. Hungría, A. Iglesias-Juez, O. Gálvez, J.A. Anderson, J.C. Conesa, J. Soria, G. Munuera, J. Catal. 214 (2003) 261–272.

[46] K. Qian, W.X. Huang, J. Fang, S.S. Lv, B. He, Z.Q. Jiang, S.Q. Wei, J. Catal. 255 (2008) 269–278.
[47] A.N. Il'ichev, A.A. Firsova, V.N. Korchak, Kinet. Catal. 47 (2006) 585–592.
[48] K.I. Hadjiivanov, G.N. Vayssilov, Adv. Catal. 47 (2002) 307–511.
[49] M.B. Padley, C.H. Rochester, G.J. Hutchings, F. King, J. Catal. 148 (1994) 438–452.
[50] J.W. Bijsterbosch, F. Kapteijn, J.A. Moulijn, J. Mol. Catal. 74 (1992) 193–205.
[51] O. Dulaurent, X. Courtois, V. Perrichon, D. Bianchi, J. Phys. Chem. B 104 (2000) 6001–6011.